

Simulation Studies on Image Reconstruction Algorithm for Portable Electrical Capacitance Tomography

A. A. Hamzah^{1,2}, R. A. Rahim^{1,3,*}, E.J. Mohamad¹, J. Pusppanathan³,
K. A. Kadir⁴, H.L.M. Ameran¹, M. N. A. Mohamed⁵

¹Faculty of Electrical and Electronic Engineering, Universiti Tun Hussein Onn, 86400 Batu Pahat, Johor

²Section of Chemical Engineering Technology, Universiti Kuala Lumpur Malaysian Institute of Chemical and Bioengineering Technology (UniKL MICET), 78000, Alor Gajah, Melaka

³Faculty of Electrical Engineering, Universiti Teknologi Malaysia, 81310, Skudai, Johor

⁴Electrical Engineering Section, UniKL BMI, Gombak, Selangor, Malaysia

⁵Centre for Language Studies, Universiti Tun Hussein Onn Malaysia, 86400 Batu Pahat, Johor

Received 14 February 2018; accepted 3 September 2018, available online 31 December 2018

Abstract: Electrical capacitance tomography (ECT) is a non-invasive and non-intrusive internal visualization tomographic modality which promises a better quantification by providing cross-sectional distribution information of any kind of multiphase flow. The studies discussed in this paper aim to investigate the non-iterative and iterative image reconstruction for 16 channels of portable electrical capacitance tomography (ECT) through simulation work. Linear Back Projection (LBP) as a non-iterative algorithm was compared with the Landweber and generalized vector sampled pattern matching (GVSPM) iterative algorithm for four cases which are core flow, annular flow, stratified flow and two circles by evaluation of percentage error and image correlation. The results show that Landweber algorithm produces lowest percentage error, higher correlation coefficient and acceptable elapsed time for all cases studied. Iterative image reconstruction will produce accurate results by eliminating the artifacts near actual object and enhance the capability of segmented ECT in multiphase flow identification.

Keyword: ECT, image reconstruction, inverse problem, iterative algorithms

1. Introduction

To date electrical capacitance tomography has been used rapidly for investigation of the complexities of multiphase flow phenomena either for lab scale equipment or industrial application such as fluidised beds [1,2], packed beds [3], pneumatic conveying in horizontal tube [4,5], crude palm oil analysis [6] and microchannel [7]. Basically, ECT consists of multiple electrodes which are placed surrounding a pipe or vessel and the capacitance value will be measured based on the different electrical permittivity of two materials inside the pipe or vessel, through data acquisition system. Then, these measurements will be used to reconstruct permittivity distribution by applying the mathematical algorithm. This technique has advantages whereby it can be operate at low cost, high speed and is non-invasive as well as non-intrusive.

The most important part of ECT is the sensor design in term of the accuracy in the measurement process. Yang 2010 [8] described in details the ECT sensor design including the number of electrodes, length of electrodes, earth screens (axial, radial and outer screen) and guard electrodes. The second part of ECT is the data acquisition system (DAS) which mainly consists of capacitance measuring circuits. Commonly, two types of DAS are used which are charge-discharge circuit and AC based because of their stray-immune. The cable connected from

the measuring sensor to the circuit, the switching system of excitation and detection mode and the outer screen are the main source of stray capacitance or inaccurate measurement [9]. The best solution is by combining the sensor with the capacitance measuring circuit [10]. This method is cable-less aiming to reduce the stray capacitance source through cable movement and its length. The last part of ECT is image reconstruction using an appropriate algorithm. The main problems with image reconstruction of ECT are ill-determined where the number of equations is less than the number of variables and ill-conditioned caused by nonlinearity behavior of the electric field. The basic most popular algorithm is linear back projection (LBP) method. This method is fast in calculation but low in accuracy. The popular iterative methods in ECT are Tikhonov regularization and Landweber iteration with promising accuracy [11]. Both of these methods depend on empirical values to reconstruct the accurate image. Takei & Saito (2004) [12] introduced generalized vector sampled pattern matching method to overcome the drawbacks of Tikhonov regularization and Landweber iteration.

This paper aims to study the image reconstruction on 16 ECT segmented electrodes by simulation works. It will cover generating sensitivity matrix, image reconstruction by non-iterative (LBP) algorithm as a

reference and iterative (Landweber and GVSPM) algorithms for four case studies or flow regimes.

2. Governing Equation

The electric field distribution and electrical potential distribution in ECT sensor can be described using Poisson equation. Since there are no sources inside the sensor, assumption charge distribution of zero was implemented [13].

$$\nabla \cdot [\varepsilon(\mathbf{r}) \nabla \phi_{ij}(\mathbf{r})] = 0 \tag{1}$$

where $\varepsilon(\mathbf{r})$ is the relative permittivity, $\phi_{ij}(\mathbf{r})$ is potential at a position (\mathbf{r}) , ∇ is the divergent operator, $\rho(\mathbf{r})$ is the charge distribution and i is the transmitter electrode while j is the receiver electrode. The measurement mode is based on a low Z-scheme method where one electrode will be a transmitter while the rest will be kept on ground potential and labelled as the receiver [14]. This method produces the total number of independent measurement, $M = N(N - 1)/2$ for the number of electrodes, N . The equations for the transmitter and the receiver are as below:

$$\text{Transmitter: } \int_i \frac{\partial \phi(\mathbf{r})}{\partial \mathbf{n}} \cdot dl_i = V_o \tag{2}$$

$$\text{Receiver: } \int_j \frac{\partial \phi(\mathbf{r})}{\partial \mathbf{n}} \cdot dl_j = 0 \tag{3}$$

where l is the length of electrode, $V_o = V \sin(2\pi ft)$ is a potential difference measurement in a specific frequency, f and amplitude, V is injected [15,16]. Lastly, the capacitance value can be measured as follows:

$$c_{ij} = -\frac{1}{V_{ij}} \int_{\mathbf{r} \in \Gamma_{ij}} \varepsilon(\mathbf{r}) \nabla \phi_{ij}(\mathbf{r}) \cdot d\mathbf{r} \tag{4}$$

where V_{ij} is the potential difference between i and j electrodes and Γ_{ij} is an area of the total capacitance for electrode ij . The configuration of ECT sensor can be seen in Fig. 1.

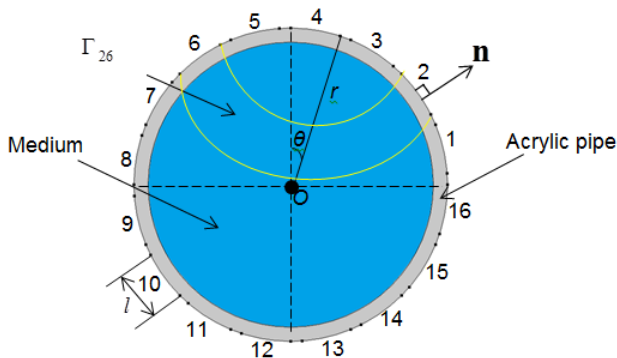


Fig. 1: ECT sensor configuration

3. Image Reconstruction

Practically, image reconstruction of ECT involves two main steps which are forward problem (capacitance determination from permittivity distribution) and the

inverse problem (permittivity distribution calculation from capacitance measurements). Capacitance can be linearized to permittivity distribution in matrix form as follows:

$$\Delta c_{ij} = \mathbf{J} \Delta \varepsilon \tag{5}$$

where \mathbf{J} is the sensitivity matrix of $M \times N$, $\Delta \varepsilon$ is the permittivity distribution of $n \times 1$ and n is the pixel number such as 64×64 grid produces 4096 pixels of a square sensor. The normalized and discrete form of equation (5) relevant for solving the forward problem can be expressed as below:

$$C = S G \tag{6}$$

where C is the normalized capacitance vector, S is the normalized sensitivity matrix and G is the normalized permittivity vector [13, 16].

Linear Back Projection

The simple and famous algorithm for solving inverse problem for image reconstruction on ECT is linear back projection (LBP). This method was first implemented by Xie et al. (1989) [18] via simulation on 8 electrode ECT. The approximation solution for equation (6) by LBP algorithm is as below:

$$G = S^T C \tag{7}$$

where S^T is the matrix transpose of sensitivity map distributions. This method is typically fast in calculating without any iteration needed and widely used in any ECT system although the accuracy is low.

Landweber

Landweber is the most famous iterative algorithm used in image reconstruction for ECT because of its accuracy, cost-effective, stability and fast convergence capability [19]. This algorithm also known as the Richardson Iteration, is a variation of steepest descent direction method for quadratic function [11], [20]. The iteration procedure follows this equation.

$$G^{k+1} = G^k + \alpha S^T [C - S G^k] \tag{8}$$

where α is the step size which is fixed for each iteration. Basically, the value of α is greater than 0 and less than 1. As an approximation, equation (9) is used to calculate the step size.

$$\alpha^k = \frac{\|S^T (C - S G^k)\|_2^2}{\|S S^T (C - S G^k)\|_2^2} \tag{9}$$

The normalized capacitance for specific electrode pair in this research is measured by applying Parallel model as below:

$$C_{ij} = \frac{c_{ij}^m - c_{ij}^L}{c_{ij}^H - c_{ij}^L} \tag{10}$$

where c_{ij}^m is the measured capacitance value for electrode pair ij , c_{ij}^L and c_{ij}^H is the capacitance measurement for electrode pair ij when the sensor is filled with low and high permittivity material respectively.

Generalized Vector Sampled Pattern Matching Method (GVSPM)

This method is commonly used to avoid dependency on the empirical value in iteration procedure. Moreover, the normalization procedure is done by dividing the capacitance measurement and sensitivity matrix calculation by their norms. This method is a bit different from other algorithms in terms of the normalization of capacitance and sensitivity matrix. The equation is as follows:

$$C' = \frac{C}{|C|}, |C| = \sqrt{c_{1,2}^2 + c_{1,3}^2 + \dots + c_{N-1,N}^2} \quad (11)$$

$$S' = \frac{S}{|S|}, |S| = \sqrt{S_1^2 + S_2^2 + \dots + S_n^2}, n = n_x \times n_y \quad (12)$$

where $|C|$ indicates the norm of capacitance measurements, $|S|$ is the norm of sensitivity matrix and n is the total number of the pixel generated for image reconstruction of permittivity distributions. This research used 64 grids for n_x and n_y contributes 4096 pixels of a square sensor. The iteration procedure follows this equation.

$$G^{k+1} = G^k - S'^T \left(\frac{S'G^k}{|S'G^k|} - C' \right) \quad (13)$$

3.1 Evaluation of algorithms

Three algorithms were selected namely LBP, Landweber and GVSPM. For evaluation purpose, two criteria were used which are percentage error, IE and correlation coefficient, CC.

$$IE = \frac{|\hat{G} - G_k|}{|\hat{G}|} \times 100 \quad (14)$$

$$CC = \frac{\sum_{i=1}^n (G_k - \bar{G}_k)(\hat{G} - \bar{\hat{G}})}{\sqrt{\sum_{i=1}^n (G_k - \bar{G}_k)^2 \sum_{i=1}^n (\hat{G} - \bar{\hat{G}})^2}} \quad (15)$$

where \hat{G} is true normalized permittivity distribution, G_k is the normalized reconstructed permittivity distribution, $\bar{\hat{G}}$ and \bar{G}_k are the mean value of \hat{G} and G_k respectively.

4. Results and Discussions

To investigate the image reconstruction performance, four permittivity distributions were chosen as shown in Fig. 2. The sensor was designed the same as the actual segmented ECT as depicted in Fig. 1 with the outer diameter of the pipe was, $D_o = 110$ mm and its thickness was, $\Delta x_{pipe} = 10$ mm. The relative permittivity of the acrylic pipe was set to, $\varepsilon_{pipe} = 2.6$ [-]. Phantom (a) was the core flow with a diameter of the core, $D_{core} = 30$ mm, composed by an acrylic rod with permittivity, $\varepsilon_{rod} = 2.6$ [-] and surrounded by air with relative permittivity,

$\varepsilon_{air} = 1.0$ [-]. Phantom (b) was the annular flow with the thickness of $\Delta x_{annular} = 20$ mm composed by an acrylic while blue color at the pipe center is air. Phantom (c) the stratified flow was set according to the half of the pipe height which acrylic at the bottom as red color and air at the top as blue color. Phantom (d) consist of two acrylic rods with diameter, $D_{2C} = 20$ mm as two circle phantom. The color scale below the phantom on Fig. 2 is normalized permittivity between air and acrylic mediums. The simulation processes were implemented using COMSOL Multiphysics and Matlab on a PC with Pentium Core-i5 and 8 Gbytes of memory.

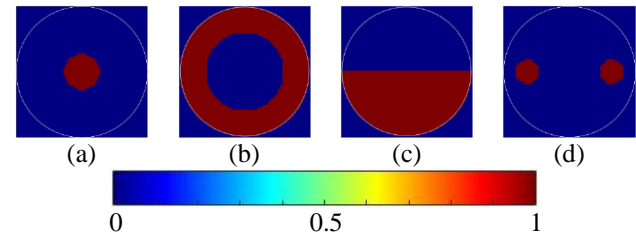


Fig. 2: Phantom conditions

Fig. 3 shows the normalized permittivity, G where the values are in the range of 0 to 1, reconstructed by LBP, Landweber and GVSPM algorithms and compared to actual conditions for four cases. The number of iteration was set to 500 for both iterative algorithms with the step size of 0.13 for Landweber. The color scale at the bottom is normalized permittivity between air and acrylic mediums. As expected, Figure 3 shows that iterative algorithms produce better images than non-iterative. The black circle and line show the actual position and size of the phantoms. LBP gives a moderate image for Phantom (a) with more artifacts around the acrylic pipe, while Landweber gives slightly fewer artifacts than GVSPM method. Both methods are still acceptable. Phantom (b) shows inaccurate results for all algorithms with more artifacts on LBP and smaller size of annular for Landweber and GVSPM compared to the actual phantom. Phantom (c) shows that Landweber and GVSPM generate nearly same results while LBP generates the same pattern with iterative algorithms. Landweber shows fewer artifacts with the two circles located in the best position compared to GVSPM, while LBP produces more artifacts around the two circles of phantom (d) compared to GVSPM.

Table 1 shows the percentage error of reconstructed image by LBP, Landweber and GVSPM relative to actual simulation conditions. For all cases, Landweber algorithm produces superior results based on the low percentage error while LBP produces the highest and GVSPM produces acceptable value. These results correspond to the best images in Figure 3. Table 2 shows how similar are the images generated by each algorithm using correlation coefficient parameter. The highest value is the best in terms of producing accurate image reconstruction. With respect to the lowest percentage error in Table 1, Landweber algorithms produce the highest value especially for phantom (a) and (d) while the value is just

enough for phantom (b) and (c). GVSPM algorithms show tolerable value for correlation coefficient which is quite close to Landweber while the moderate value is gained from LBP algorithms. In order to compare the speed of the algorithms in generating images, elapsed time was recorded via Matlab function as shown in Table 3. LBP produces the fastest in generating images because no iteration is involved while iterative algorithms need more than 1 second for 500 iterations. There is no significant difference between Landweber and GVSPM, indicating that both algorithms is possible to be used for the online application.

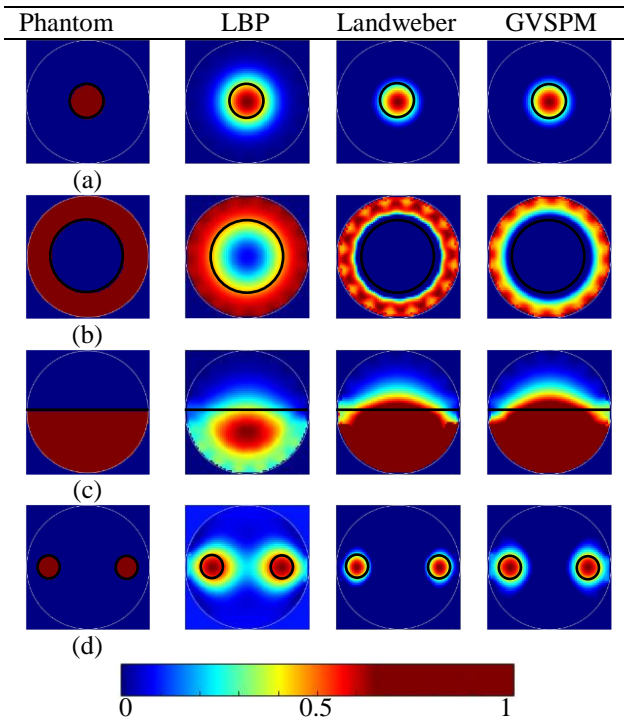


Fig. 3: Image reconstruction based on simulated data

Table 1: Percentage error (%)

	(a)	(b)	(c)	(d)
LBP	45.90	45.20	37.64	83.82
Landweber	24.31	29.85	23.08	35.68
GVSPM	30.00	31.99	30.59	58.52

Table 2: Correlation coefficient

	(a)	(b)	(c)	(d)
LBP	0.74	0.36	0.66	0.45
Landweber	0.90	0.72	0.77	0.87
GVSPM	0.89	0.68	0.67	0.75

Table 3: Elapsed time, $t(s)$

	(a)	(b)	(c)	(d)
LBP	0.06	0.06	0.06	0.06
Landweber	0.99	0.99	1.01	1.02
GVSPM	1.19	1.15	1.25	1.11

Currently, 16 segmented ECT implemented LBP algorithm to visualize multiphase flow in the piping system. This research introduced iterative algorithms to

enhance the accuracy of data measurement. Accurate image reconstruction is a crucial part of ECT for concentration analysis, flow pattern recognition and velocity distributions. The main problem with iterative algorithm implementation in ECT system is the time required to perform each iteration. To overcome this drawback, improvements in conditioning circuit is required such as the application of FPGA [22–24].

The results obtained show that Landweber iteration is superior than GVSPM and LBP methods. The limitation of Landweber is the step size selection which is a vital parameter in simulation process. With the low value (close to zero), this method requires more iteration number while big number (close to 1) will produce non-convergent simulation. Liu [24] used updated step size instead of remains constant to solve this issue and improve the accuracy with less time consuming for Landweber iteration method.

5. Conclusions

The non-iterative and iterative image reconstructions have been applied to solve the ill-posed inverse problem on electrical capacitance tomography for gas-solid two-phase flow namely LBP, Landweber and GVSPM. 16 segmented ECT was applied successfully to four types of phantom conditions which are core flow, annular flow, stratified flow and two circles indicating the dispersion concentration of material inside the pipe. Based on the image analysis, Landweber algorithm shows the best results compared to others in terms of image accuracy, low percentage error and higher correlation coefficient with acceptable elapsed time. These results are the stepping stone to improve the current 16 segmented ECT as a portable measurement device to produce more accurate results in terms of visualization.

References

- [1] Liu, S., Chen, Q., Wang, H. G., Jiang, F., Ismail, I., Yang, W. Q. (2005). Electrical capacitance tomography for gas-solids flow measurement for circulating fluidized beds. *Flow Measurement & Instrumentation*. 16(2-3): 135–144.
- [2] Makkawi, Y. T., Wright, P. C. (2004). Electrical capacitance tomography for conventional fluidized bed measurements - Remarks on the measuring technique. *Powder Technology*. 148(2-3): 142–157.
- [3] Hamidipour, M., Larachi, F. (2010). Characterizing the liquid dynamics in cocurrent gas-liquid flows in porous media using twin-plane electrical capacitance tomography. *Chemical Engineering Journal*. 165(1): 310–323.
- [4] Cong, X., Guo, X., Lu, H., Gong, X., Liu, K., Sun, X., Xie, K. (2013). Flow patterns of pulverized coal pneumatic conveying and time-series analysis of pressure fluctuations. *Chemical Engineering Science*. 101:303–314.
- [5] Cong, X., Guo, X., Gong, X., Lu, H., Dong, W. (2011). Experimental research of flow patterns and

- pressure signals in horizontal dense phase pneumatic conveying of pulverized coal. *Powder Technology*. 208(3):600–609.
- [6] Mohamad, E.J., Rahim, R.A., Rahiman, M. H. F., Ameran, H. L. M., Wahab, Y. A., Marwah, O. M. F. (2016). Analysis of crude palm oil composition in a chemical process conveyor using Electrical Capacitance Tomography. *Flow Measurement Instrumentation*. 50:57–64.
- [7] Ali Othman, N. T., Obara, H., Sapkota, A., Takei, M. (2015). Measurement of particle migration in micro-channel by multi-capacitance sensing method. *Flow Measurement & Instrumentation*. 45: 162–169.
- [8] Yang, W. (2010). Design of electrical capacitance tomography sensors. *Measurement Science Technology*. 21(4):42001.
- [9] Yang, W. Q. (1996). Hardware design of electrical capacitance tomography systems. *Measurement Science Technology*. 7:225–232.
- [10] Wan Norhisyam Abd Rashid, Elmy Johana Mohamad, Ruzairi Abdul Rahim, Jaafar Abdullah, Hanis Liyana Mohamad Ameran, (2016). Electrical capacitance tomography: a review on portable ECT system and hardware design. *Sensor Review*. 36(1):64–70.
- [11] Yang, W. Q., Peng, L. (2002). Image reconstruction algorithms for electrical capacitance tomography. *Measurement Science Technology*. 14(1):1–13.
- [12] Takei, M., Saito, Y. (2004). Application of the generalized vector sampled pattern matching method to reconstruction of electrical capacitance CT images. 15:1371–1381.
- [13] Kim, Y. S., Lee, S. H., Ijaz, U. Z., Kim, K. Y., Choi, B. Y. (2007). Sensitivity map generation in electrical capacitance tomography using mixed normalization models. *Measurement Science Technology*. 18(7):2092–2102.
- [14] Neumayer, A., Zangl, M., Watzenig, H., Fuchs, D., (2011). *New Developments and Applications in Sensing Technology*. Springer. 65-106.
- [15] Baidillah, M. R., Takei, M. (2017). Exponential model normalization for electrical capacitance tomography with external electrodes under gap permittivity conditions. *Measurement Science and Technology*. 28:64002-64015.
- [16] Xie, C. G. G., Huang, S. M. M., Beck, M. S. S., Hoyle, B. S. S., Thorn, R., Lenn, C., Snowden, D., Beck, M. S. S. (1992). Electrical capacitance tomography for flow imaging: system model for development of image reconstruction algorithms and design of primary sensors. *IEE Proceedings G Circuits, Devices and Systems*. 139(1):89–98.
- [17] Li, K. (2015). A Brief Survey of Image Processing Algorithms in Electrical Capacitance Tomography. 1–10.
- [18] Xie, C. G., Plaskowski, A., Beck, M. S. (1989). 8-electrode capacitance system for two-component flow identification. Part 1: Tomographic flow imaging. *IEEE Proceedings A (Physical Science, Measurement and Instrumentation, Management and Education)*. 136(4):173–183.
- [19] Liu, X., Wang, X., Hu, H., Li, L., Yang, X. (2015). An extreme learning machine combined with Landweber iteration algorithm for the inverse problem of electrical capacitance tomography. *Flow Measurement Instrumentation*. 45:348–356.
- [20] Byrne, C. L. (2006). *Iterative Algorithms in Inverse Problems*. UMass Library.
- [21] Deabes, W. A., Abdallah, M., Elkeelany, O., Abdelrahman, M. A. (2009). Reconfigurable wireless stand-alone platform for electrical capacitance tomography. *IEEE Symposium on Computational Intelligence in Control and Automation, CICA 2009 – Proceedings*. 112–116.
- [22] Cui, Z., Wang, H., Yang, C., Zhang, D., Geng, Y. (2012). Development and application of ECT digital system for online flow measurement. *IST 2012 - 2012 IEEE International Conference on Imaging Systems and Techniques, Proceedings*. 599–604.
- [23] Herdian, H., Muttakin, I., Saputra, A., Yusuf, A., Widada, W., Taruno, W. P. (2016). Hardware implementation of linear back-projection algorithm for capacitance tomography. *Proceedings - 4th International Conference on Instrumentation, Communications, Information Technology and Biomedical Engineering, ICICI-BME*. 124–129.
- [24] Liu, S., Fu, L., Yang, W. Q. (1999). Optimization of an iterative image reconstruction algorithm for electrical capacitance tomography. *Measurement Science Technology*. 10(7): L37–L39.